ANNALI DI GEOFISICA, VOL. 41, N. 5-6, November-December 1998

Ionospheric drift measurements with ionosondes

Bodo W. Reinisch, James L. Scali and D. Mark Haines
Center for Atmospheric Research, University of Massachusetts Lowell, MA 01854, U.S.A.

Abstract
In the last forty years many attempts have been made to measure ionospheric plasma motions with HF radio sounders, generally specialized ionosondes. Starting in the 1950's, the so-called similar fading and the correlation methods were applied to estimate the velocities in the ionosphere. More recently, the interferometric Doppler technique was introduced which successfully measured ionospheric drifts that were verified by incoherent scatter radar measurements. The latter technique is discussed in some detail in this paper.

Key words *ionospheric drift – Doppler interferometry – ionosonde – digisonde – skymap*

1. Introduction

Modern ionosondes operate like High Frequency (HF) Doppler radar systems measuring echo amplitude and phase, angle of arrival, polarization, and Doppler spectrum as a function of range. Digital operations control and real time signal processing make it possible to operate such HF radar systems in a variety of modes supporting different applications: routine ionospheric sounding, real-time frequency management, channel probing, and ionospheric structure and dynamics research (Reinisch *et al.*, 1997). Of special importance for this paper is the interferometric Doppler technique that is currently being used to measure ionospheric drifts. Most conventional ionosondes developed from the 1940's to the 1970's were rather simple instruments that measured at best echo amplitude as a function of range and frequency. Nevertheless, by receiving the ionospherically reflected signals at three or more spaced antennas, about one wavelength apart, and comparing the measured amplitude fluctuations it became possible to obtain estimates of the direction and speed of ionospheric motions applying similar fading or correlation analysis.

Mailing address: Prof. Bodo W. Reinisch, Center for Atmospheric Research, University of Massachusetts-Lowell, 600 Suffolk Street, Lowell, MA 01854, U.S.A.; e-mail: Bodo_Reinisch@uml.edu

2. Similar fading and correlation methods

Fifty years ago, Mitra (1949) introduced radio drift measurements using frequencies of a few megahertz and three spaced antennas (O, X, Y) arranged in a rectangular triangle. The time delays, t_x and t_y, of certain discernible amplitude features recognized at the three antenna locations are related to the speed v and the direction α with respect to the x-axis by

$$t_x = (OX \cos \alpha)/v, \qquad t_y = (OY \sin \alpha)/v \quad (2.1)$$

where OX and OY are the respective antenna distances (Krautkrämer, 1950). In principle v and α can easily be calculated from (2.1), but there are difficulties in interpreting the meaning of v for a number of reasons. The amplitude fading patterns on the ground are produced by interfering echoes reflected at irregularities in the ionosphere, and the theory predicts that the

fading pattern on the ground moves with twice the velocity of the irregularities, *i.e.* $v = 2v_D$. Most of the early radio drift measurements were made in the E region, where the neutral wind and plasma drift are tightly coupled. Comparison with neutral wind velocities indicated that approximately $v = v_D$, and not $v = 2v_D$. The fact that the irregularity structures vary while they move over the station complicates the interpretation of the moving fading patterns (Harnischmacher and Rawer, 1958).

The simple fading analysis was superceded by the more elaborate correlation analysis techniques using time and spatial correlation functions that take into account the changing patterns during the measurement period (Briggs *et al.*, 1950; Phillips and Spencer, 1955). The full correlation analysis derives the translational velocity v and a characteristic «random velocity» v_C. Comparison with the simple fading analysis indicates that the similar fading method overestimates v (Fooks and Jones, 1961; Rawer, 1963). In the 1970's the interest in E and F region drift measurements with vertical HF sounding started to decline, and there are two reasons for this. The powerful Incoherent Scatter Radar (ISR) facilities measured ionospheric drifts with high resolution, and the HF drift measurements were not or could not be validated by the ISR observations. In contrast, oblique sounding at frequencies below 1 MHz for the measurement of D region velocities continued to deliver reliable results (Sprenger and Schminder, 1967; Jacobi *et al.*, 1997; Jacobi *et al.*, 1998). The emergence of the modern digital ionosonde in the last two decades offered exciting new possibilities of measuring ionospheric motions and the $\boldsymbol{E}\times\boldsymbol{B}$ drifts. A review of ionospheric drift measurements by Rawer (1993) summarizes the features of the similar fading and correlation methods but does not discuss the modern techniques.

3. Modern drift measurements using Doppler interferometry

After Pfister (1974) suggested the use of HF phase measurements and spectral analysis in ionospheric sounding, new digital ionosondes were developed that measured the amplitude and phase of all echoes and calculated the complex spectra of all echo returns (Bibl and Reinisch, 1978; Hunsucker, 1991). One of these modern ionosondes, the Digisonde Portable Sounder or DPS (Haines, 1994; Reinisch, 1996) is operated today in Rome, Italy, by the institute that Pietro Dominici had led for so many years (http://digisonde.ingrm.it/).

In contrast to incoherent or coherent scatter radar systems which observe backscattered radio energy, ionosonde sounding is based on total (specular) reflection which occurs at the level where the wave frequency f is equal to the plasmar frequency f_p (for the ordinary polarization). In general, the transmit antenna has a wide radiation pattern and illuminates a large area in the ionosphere with a diameter of several hundred kilometers, either the E or the F layer dependent on frequency. If the ionosphere is perfectly stratified, most of the energy is reflected away and only one echo is received from the point where the normal of the plasma frequency contour $f_p = f$ is parallel to the wave normal of the incident wave. In the presence of undulated contours and irregularities many echoes will return to the ionosonde's receiving antennas as illustrated in fig. 1. All echoes with pulse propagation times that differ by less than the pulse width will superimpose forming a composite signal at the antennas. Assuming a 33 μs pulse width and a virtual height of 300 km this means that echoes from within a cone of 10° overlap; this angle becomes 15° for a 66 μs pulse. If the ionospheric structure is moving with a velocity $\boldsymbol{v}_D$, each echo will have its characteristic Doppler frequency shift d_i

$$d_i = \frac{1}{\pi}\boldsymbol{k}_i \cdot \boldsymbol{v}_D = \frac{2}{\lambda} v_{\mathrm{los},i} \qquad (3.1)$$

where $\boldsymbol{k}_i$ is the wave vector of ith echo, and $v_{\mathrm{los},i}$ the line-of-site (los) velocity of the ith reflector or echo «source». To decompose the signal into its Doppler components, the DPS performs at each height range a Fast Fourier Transform (FFT) for each antenna signal. Once the interfering echo waves are spectrally separated, interferometry can determine the angle of arrival

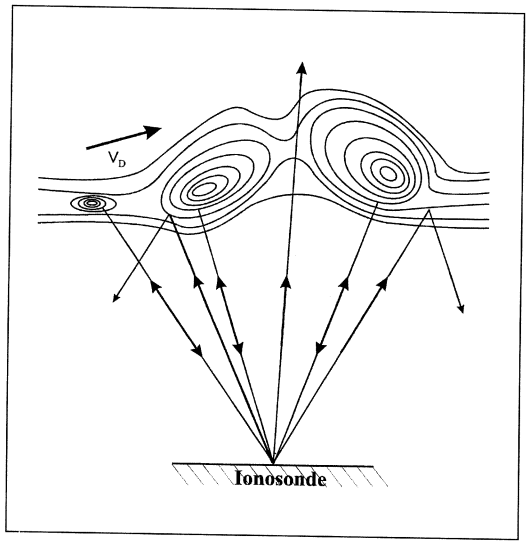

Fig. 1. Multiple HF echoes from a structural ionosphere. Each returning echo has a different Doppler frequency shift if the structure moves with velocity $\boldsymbol{v}_D$.

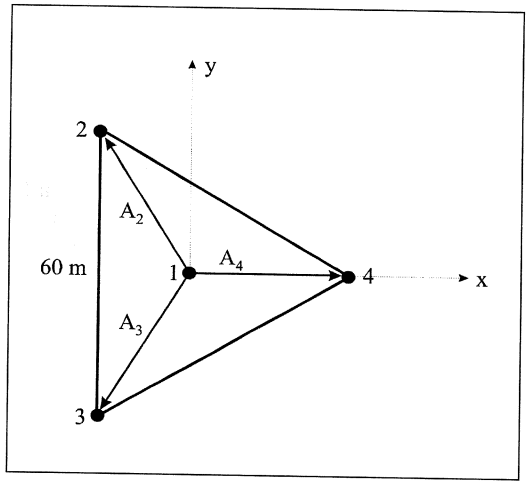

Fig. 2. Triangular arrangement of four receiving antennas for interferometry measurements. Each of the four antennas is circularly polarized to distinguish between ordinary and extraordinary polarized echoes. $\boldsymbol{A}_2$, $\boldsymbol{A}_3$, and $\boldsymbol{A}_4$ are vectors from antenna 1 to antennas 2, 3, and 4.

(AOA) of each echo. The DPS uses four small circularly polarized crossed-loop antennas for reception, three at the corners of an equilateral triangle with a base-length of 60 m, and a fourth at the center of the triangle as shown in fig. 2. A plane wave with a wave normal $\boldsymbol{n}_i$, specified by its zenith angle θ_i and azimuth angle ϕ_i, produces the phase difference $\Delta_{m,i}$ with respect to antenna 1

$$\Delta_{m,i} = \frac{2\pi}{\lambda} \boldsymbol{A}_m \cdot \boldsymbol{n}_i \quad m = 2,3,4 \quad i = 1,2,3,\ldots..I \tag{3.2a}$$

$$\Delta_{m,i} = \frac{2\pi}{\lambda} \boldsymbol{A}_m \cdot (\boldsymbol{a}_x \cos\varphi_i \sin\theta_i + \boldsymbol{a}_y \sin\varphi_i \cos\theta_i + \boldsymbol{a}_z \cos\theta_i) \tag{3.2b}$$

where I is the total number of sources. The antenna location vectors $\boldsymbol{A}_m$ with respect to the x (east), y (north) and z (vertical) axes are

$$\boldsymbol{A}_2 = A(-\cos 60°, \sin 60°, 0),$$

$$\boldsymbol{A}_3 = A(-\cos 60°, -\sin 60°, 0),$$

$$\boldsymbol{A}_4 = A(1, 0, 0), \qquad A = (60/\sqrt{3})m.$$

The wave vectors $\boldsymbol{k}_i = (2\pi/\lambda)\,\boldsymbol{n}_i$ can be found by solving (3.2b) for ϕ_i and θ_i. For each source i there are three equations to solve for the two unknowns θ_i and ϕ_i. This makes it possible to check whether the wave has a plane wave front which requires

$$\sum_{m=2}^{4} \Delta_{m,i} = 0. \tag{3.3}$$

When each detected source with its los velocity is presented in a θ, ϕ diagram one obtains a skymap reminiscent of an optical all-sky image. A typical example of a skymap is shown in fig. 3 for a 20 s night measurement at 2.8 MHz at Millstone Hill (42°N geogr.). At this time all echoes arrived from the north and the los velocities indicate a westward motion of the plasma.

At this point, the results resemble those of a Doppler radar that has measured the los veloci-

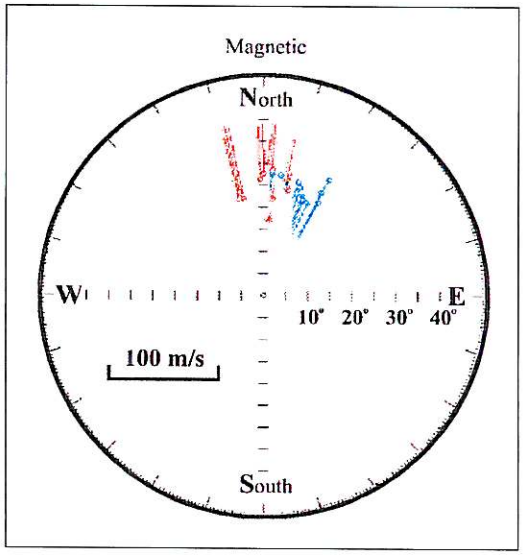

Fig. 3. HF skymap obtained from Millstone Hill Digisonde data. All echo sources (circles) lie in the north. The los velocities are proportional to the length of the bars. Positive and negative Doppler shifts are shown in red and blue.

ties in many different directions. In principle it suffices to select any three spatially separated sources and find $\boldsymbol{v}_D = (v_x, v_y, v_z)$ from (3.1) considering that $v_{los} = \boldsymbol{n}_i \cdot \boldsymbol{v}_D$

$$\frac{1}{2}\lambda d_i = v_x \cos\phi_i \sin\theta_i + \\ + v_i \sin\phi_i \sin\theta_i + v_z \cos\theta_i \quad i = 1, 2, 3. \tag{3.4}$$

4. Calculating drift velocities with DDA

To obtain a valid velocity from (3.4), the three sources must move with the same velocity. This will be the case only when a uniform velocity $\boldsymbol{v}_D$ exists within the view of the sounder, and any three (non-collinear) sources will produce the same or similar results depending on the signal-to-noise ratio. In this situation, the translational velocity (v_x, v_y, v_z) can be found by least-squares fitting using all the skymap points

$$\varepsilon^2 = \sum_i^I [\frac{1}{2}\lambda d_i - (v_x \cos\phi_i \sin\theta_i + \\ + v_y \sin\phi_i \sin\theta_i + v_z \cos\theta_i)]^2 . \tag{4.1}$$

This method, which assumes a uniform velocity, was applied in all the early Digisonde Drift Analysis (DDA) (Reinisch *et al.*, 1987; Cannon *et al.*, 1991; Smith *et al.*, 1998) generating reliable plasma drift data for the high latitude ionosphere. Scali *et al.* (1995) used this technique and compared the resulting *F* region drifts at Sondrestromfjord (76°N CGL) with the results from the co-located Incoherent Scatter Radar (ISR). Figure 4 shows the drifts for a 24 h period, averaged over five days, obtained from the two instruments. The eastward velocity perpendicular to the magnetic field, v_{pE}, is displayed on top, and the northward component, v_{pN}, below. There is very good agreement between the two drift techniques, with noticeable differences, however, at certain times. We have analyzed the observations at these times and identified the following causes for the differences:

1) The velocity is not uniform within the field of view.

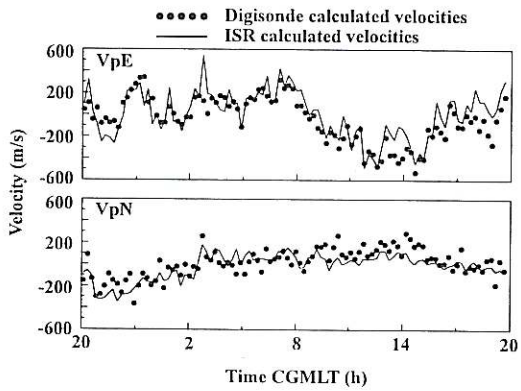

Fig. 4. *F* region drift velocities at Sondrestromfjord for 24 h; 5-day average (5-9 December 1991) for the eastward and northward velocity components. The solid line represents the ISR velocities, the dots are the Digisonde velocities.

2) The velocity is not stationary during the measurement.

3) Spectral aliasing in the Fourier transform.

The techniques by either instrument are prone to calculate erroneous velocities from (3.4) when the velocity is not uniform (problem 1). This situation occurred from 13 to 15 CGMLT (Corrected Geomagnetic Local Time) when the station was crossing the velocity reversal boundary of the polar convection cells (Heppner and Maynard, 1987), and some ionospheric sources may have been in the sunward, others in the anti-sunward flow. The Generalized Digisonde Drift Analysis (GDDA), discussed

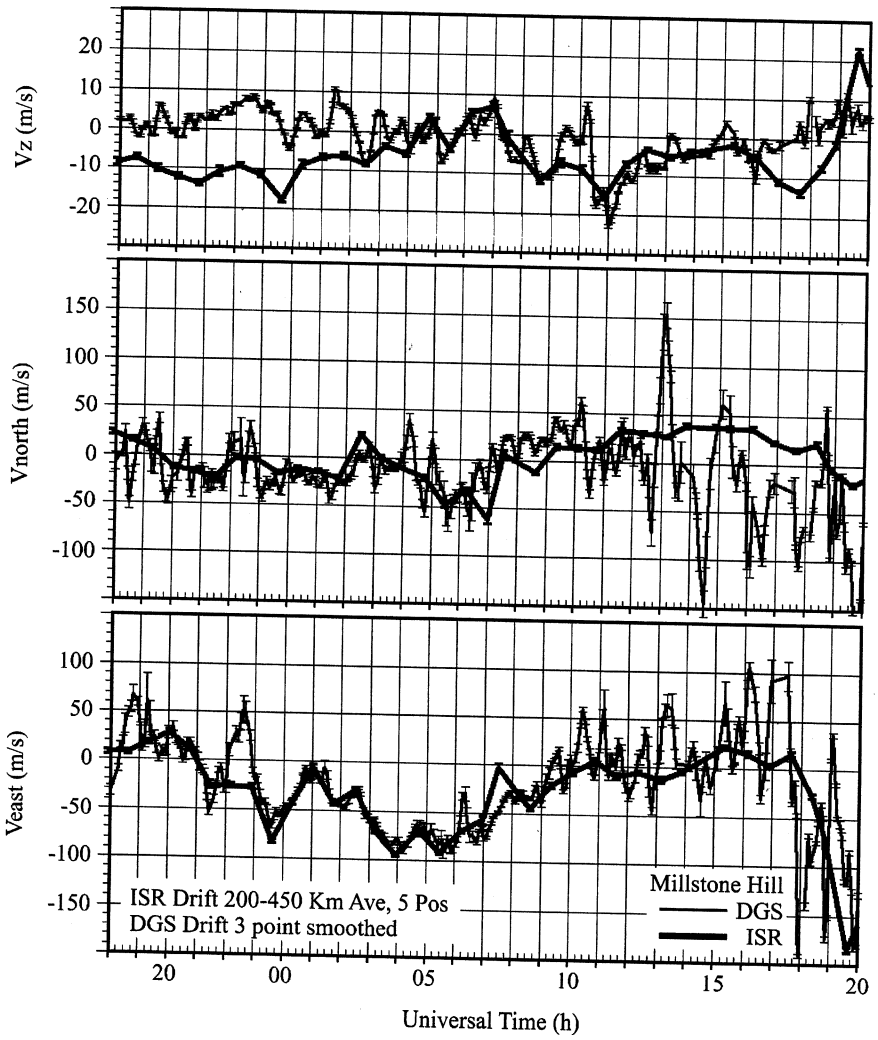

Fig. 5. Comparison of the *F*-region plasma drift at Millstone Hill as measured by the ISR (thick line) and Digisonde (thin line). The ISR is calculated from 5 antenna positions averaged from 200-450 km. The DGS drift is smoothed with a 3 point binomial smoothing function. 07-08 March 1989. (Reproduced from Bullett, 1994).

below, is able to resolve several velocities using the many simultaneous sources. The ISR can also resolve different velocities by steering the antenna dish in more than three different directions and assessing the observed los velocities; these measurements are done sequentially and therefore require a longer time which may cause problems in the presence of time-varying velocities (problem 2). The time resolution of the Digisonde, on the other hand, is very high since complete skymaps are obtained every 5 s. Problem 3 can occur in the presence of high ve-

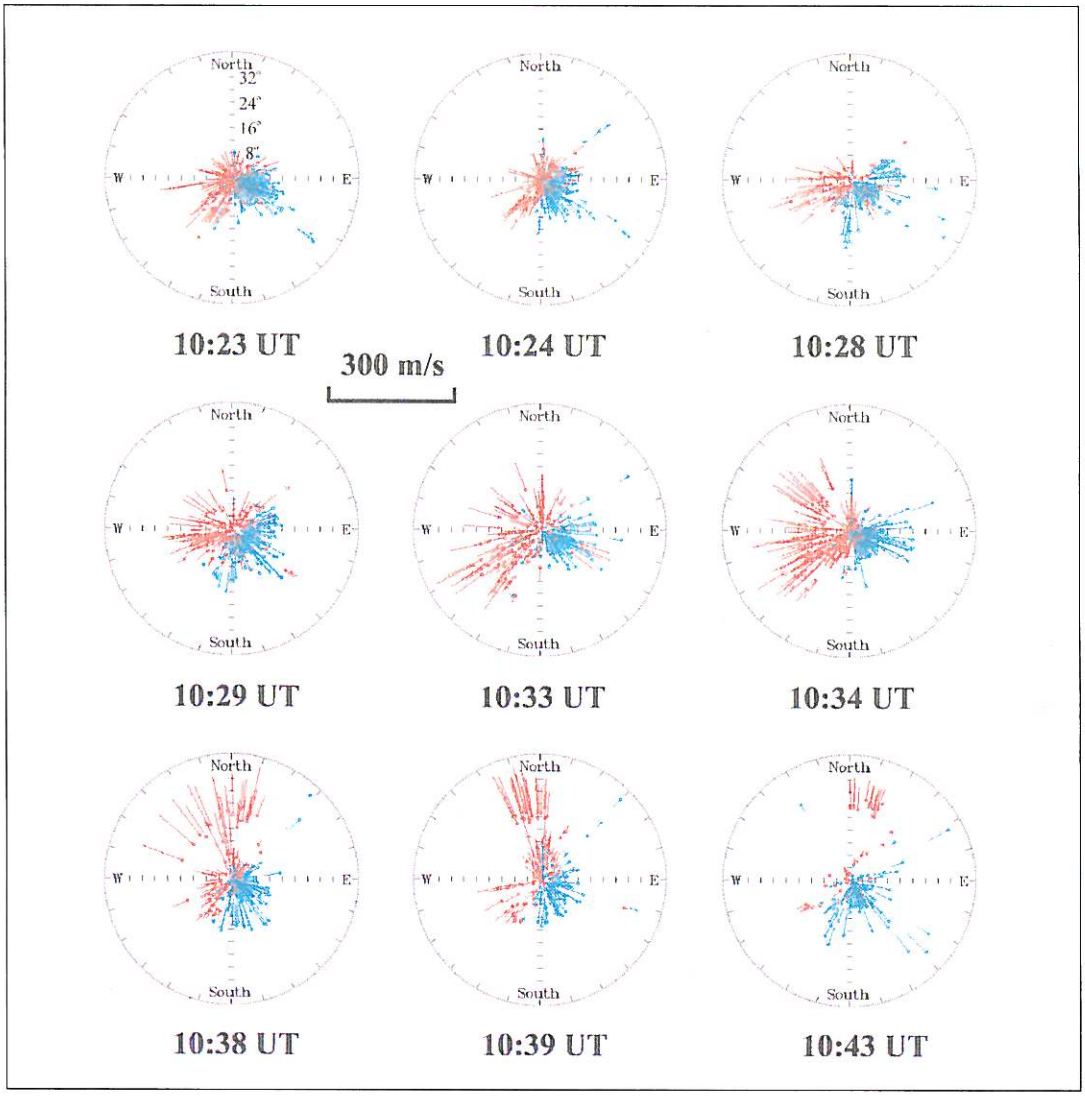

Fig. 6. Sequence of skymaps from Digisonde measurements in the polar cap at Qaanaaq on 29 March 1992 showing an *F* region patch moving over the station.

locities. It is likely that under-sampling resulted in frequency aliasing causing the low values of the Digisonde velocities at 0330 CGMLT.

Bullett (1994) compared the HF Doppler interferometric drifts at Millstone Hill, a mid latitude station, with the drifts derived from or co-located ISR measurements (fig. 5). He found the agreement to be generally good at night, with differences observed when gravity wave drive Traveling Ionospheric Disturbances (TID's) dominated the HF Doppler shifts. During the daytime the sources are generally clustered around one point introducing large errors when v_D is calculated from (4.1). Additional errors are introduced during non-equilibrium conditions when $\delta N/\delta t$ along the wave path introduces apparent Doppler shifts (Davies, 1990). At high latitudes, ionospheric irregularities exist most of the time creating adequate angular spread between the sources, and the $\boldsymbol{E}\times\boldsymbol{B}$ drift velocity is generally larger than the TID wave velocity. This results in better agreement between ISR and HF Doppler interferometry.

5. Calculating drift velocities with GDDA

In the presence of velocity shears, analysis of skymap data must be done differently from the method described by (4.1). Instead, the «Generalized Digisonde Drift Analysis» (GDDA) should be used. As illustrated in the sequence of skymaps in fig. 6, each skymap generally contains a large number of sources. Any three separated sources within a skymap with their los velocities give the plasma velocity, as long as all three move with the same velocity. Since it is not known *a priori* which sources move with the same velocity it is necessary to try all combinations of three sources and inspect the resulting velocity distribution (Guo *et al.*, 1993). All combinations for which the three points move with the same velocity will produce the same or similar velocity values depending on the signal-to-noise ratio, and the number of occurrences of this value will show a peak. The example in fig. 7 (lower part) shows the probability distribution for the three velocity components vertical, north-south, east-west obtained from a 5 s Digisonde *F* region measurement at Sondrestromfjord. The top of the figure shows the drift velocities measured at Qaanaaq and Sondrestromfjord during a 24 h rotation of the stations around the corrected geomagnetic pole. Superimposed on the measurements is a modeled two-cell convection pattern for southward B_z. The measurements used for the plots below were made when Sondrestromfjord was at the tip of the arrow, which is the region of the velocity inversion

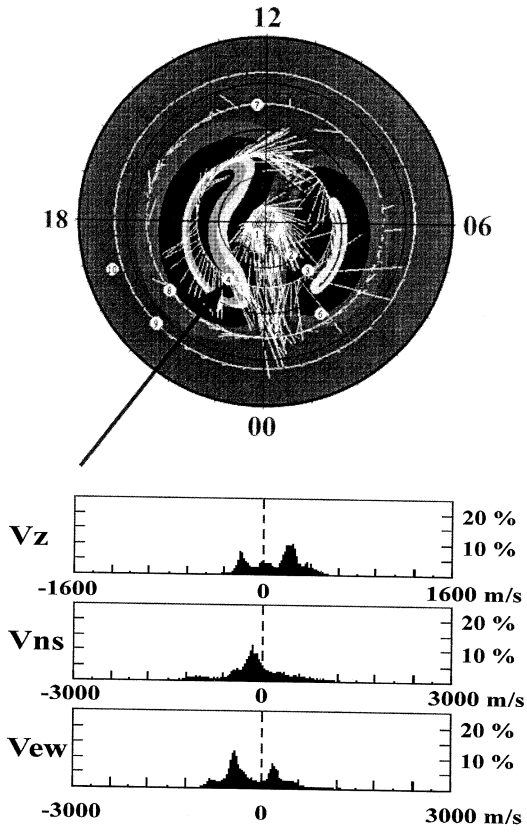

Fig. 7. Velocity shears observed at Sondrestromfjord. The polar plot on top shows 24 h of drift velocities at Qaanaaq (station 1) and Sondrestromfjord (station 4) for 8 December 1991. The plots below show the velocity probability distributions obtained from one 5 s measurement at Sondrestromfjord when the station was crossing the velocity reversal boundary (large arrow).

boundary. The sounder detected two different flows, one having a 300 m/s westward component and the other a 100 m/s eastward component. In all situations where velocity shears or curls are expected, the GDDA method will give more reliable results.

6. Summary

Ionospheric drift measurements with HF sounders provide a powerful technique for the global monitoring of ionospheric motions. Modern sounders measure the angle of arrival and the Doppler spectra of ionospherically reflected signals. This radar technique makes it possible to apply Doppler interferometry for the measurement of plasma velocities, replacing the older similar fading and correlation methods.

Acknowledgements

This work was in part supported by the Air Force Research Laboratory under contract F19628-96-C-0159.

REFERENCES

BIBL, K. and B.W. REINISCH (1978): The universal digital ionosonde, *Radio Sci.*, **13**, 519-530.

BULLETT, T.W. (1994): Mid-latitude ionospheric plasma drift: a comparison of digital ionosonde and incoherent scatter radar measurements at Millstone Hill, *Ph.D. Thesis*, University of Massachusetts, Lowell.

BRIGGS, B.H., G.J. PHILLIPS and D.E. SHINN (1950): The analysis of observations on spaced receivers of the fadings of radio signals, *Proc. Phys. Soc., London, Sect. B*, **63**, 106-121.

CANNON, P.S., B.W. REINISCH, J. BUCHAU and T.W. BULLETT (1991): Response of the polar cap *F* region convection direction to changes in the interplanetary magnetic field: digisonde measurements in Northern Greenland, *J. Geophys. Res.*, **96** (A2), 1239-1250.

DAVIES, K. (1990): *Ionospheric Radio* (Peter Peregrinus Ltd.), pp. 240.

FOOKS, G.F. and I.L. JONES (1961): Correlation analysis of the fading of radio waves, *J. Atmos. Terr. Phys.*, **20**, 229-242.

GUO, J.S., Q.W. ZHANG, H. ZHENG, C.F. XU and B.W. REINISCH (1993): Generalized digisonde drift analysis, in *Proceedings International Symposium for Radio Propagation, Beijing, China*, 699-702.

HAINES, D.M. (1994): A portable ionosonde using coherent spread-spectrum waveforms for remote sensing of the ionosphere, *Ph.D. Thesis*, University of Massachusetts, Lowell.

HARNISCHMACHER, E. and K. RAWER (1958): Drift observations evaluated by the method of similar fades, *J. Atmos. Terr. Phys.*, **13**, 1-16.

HEPPNER, J.P. and N.C. MAYNARD (1987): Empirical models of high-latitude electric fields, *J. Geophys. Res.*, **92**, 4467.

HUNSUCKER, R.D. (1991): *Radio Techniques for Probing the Terrestrial Ionosphere* (Springer Verlag), chapt. 3.3, 77.

JACOBI, C., R. SCHMINDER and D. KURSCHNER (1997): Measurements of mesopause region winds over Central Europe from 1983 through 1995 at Collm, Germany, *Beitr. Phys. Atmosph.*, 189-200.

JACOBI, C., R. SCHMINDER and D. KÜRSCHNER (1998): Planetary wave activity obtained from long-period (2-18 days) variations of mesopause region winds over Central Europe (52°N, 15°E), *J. Atmos. Terr. Solar Phys.*, **60** (1), 81-83.

KRAUTKRÄMER, J. (1950): Windmessungen in der Ionosphäre, *Arch. Elektr. Übertragungen*, **4**, 133-141.

MITRA, S.N. (1949): A radio method of measuring winds in the ionosphere, *Proc. Inst. Electr. Eng.*, Part 3, **96**, 441-446.

PFISTER, W. (1974): Drift measurements with spectral analysis during periods of chemical releases into the ionosphere, in *Methods of Measurements and Results of Lower Ionosphere Structure*, edited by K. RAWER (Akademie, Verlag, Berlin) 401-406.

PHILLIPS, G.J. and M. SPENCER (1955): The effects of anisometric amplitude patterns in the measurements of ionospheric drifts, *Proc. Phys. Soc., London, Sect. B*, **68**, 481-492.

RAWER, K. (1963): Ionospheric irregularities and movements, in *Proceedings International Conference Ionosphere*, Institute of Physics and Physical Society London, 239-251.

RAWER, K. (1993): *Wave propagation in the Ionosphere* (Kluwer Academic Publishers), pp. 200.

REINISCH, B.W. (1996): Modern ionosondes, in *Modern Ionospheric Science*, edited by H. KOHL, R. RUSTER and K. SCHLEGEL, 440-456.

REINISCH, B.W., J. BUCHAU and E.J. WEBER (1987): Digital ionosonde observations of the polar cap *F* region convection, *Phys. Scr.*, **36**, 372-377.

REINISCH, B.W., D.M. HAINES, K. BIBL, I. GALKIN, X. HUANG, D.F. KITROSSER, G.S. SALES and J.L. SCALI (1997): Ionospheric sounding in support of OTH radar, *Radio Sci.*, **32** (4), 1681-1694.

SCALI, J.L., B.W. REINISCH, C.J. HEINSELMAN and T.W. BULLETT (1995): Coordinate digisonde and incoherent scatter radar *F*-region drift measurements at Sondre Stromfjord, *Radio Sci.*, **30** (5), 1481-1498.

SMITH, P.R., P.L. DYSON, D.P. MONSELESAN and R.J. MORRIS (1998): Ionospheric convection at Casey, a southern polar cap station, *J. Geophys. Res.*, **103** (A2), 2209-2218.

SPRENGER, K. and R. SCHMINDER (1967): Results of ten years' ionospheric drift measurements in the LF range, *J. Atmos. Terr. Phys.*, **29**, 183-199.